







Nonlinear electronic stopping of negatively charged particles in liquid water

Natalia E. Koval ^{1,2,*} Fabiana Da Pieve ^{3,†} Bin Gu ^{4,5} Daniel Muñoz-Santiburcio ⁶
Jorge Kohanoff ^{4,6} and Emilio Artacho ^{1,7,8,9}

¹*CIC Nanogune BRTA, 20018 Donostia-San Sebastián, Spain*

²*Centro de Física de Materiales CFM-MPC, 20018 Donostia-San Sebastián, Spain*

³*Royal Belgian Institute for Space Aeronomy, 1180 Brussels, Belgium*

⁴*Atomistic Simulation Centre, Queen's University Belfast, Belfast BT7 1NN, Northern Ireland, United Kingdom*


⁵*Department of Physics, Nanjing University of Information Science and Technology, 210044 Nanjing, China*

⁶*Instituto de Fusión Nuclear "Guillermo Velarde," Universidad Politécnica de Madrid, 28006 Madrid, Spain*

⁷*Donostia International Physics Center DIPC, 20018 Donostia-San Sebastián, Spain*

⁸*Theory of Condensed Matter, Cavendish Laboratory, University of Cambridge, J. J. Thomson Avenue, Cambridge CB3 0HE, United Kingdom*

⁹*Ikerbasque, Basque Foundation for Science, 48011 Bilbao, Spain*

 (Received 24 February 2023; accepted 6 July 2023; published 31 July 2023)

We present real-time time-dependent density-functional-theory calculations of the electronic stopping power for negative and positive projectiles (electrons, protons, antiprotons, and muons) moving through liquid water. After correction for finite mass effects, the nonlinear stopping power obtained in this paper is significantly different from the previously known results from semiempirical calculations based on the dielectric response formalism. Linear-nonlinear discrepancies are found both in the maximum value of the stopping power and the Bragg peak's position. Our results indicate the importance of the nonlinear description of electronic processes, particularly, for electron projectiles, which are modeled here as classical point charges. Our findings also confirm the expectation that the quantum nature of the electron projectile should substantially influence the stopping power around the Bragg peak and below.

DOI: [10.1103/PhysRevResearch.5.033063](https://doi.org/10.1103/PhysRevResearch.5.033063)

I. INTRODUCTION

The problem of electronic stopping of charged particles in matter is of continuing interest in fundamental science and in many applied research areas. In particular, an accurate description of the damage caused by energetic protons and electrons in biological tissue is crucial for hadron radiotherapy of cancer [1,2] and space exploration [3–6]. The effect of ionizing radiation on the DNA components, the main subject of radiobiology, is an active field of research in which the electronic effects are yet to be understood [7].

An energetic particle moving through biological matter continually transfers energy to the target nuclei and electrons. The rate at which the projectile loses energy to the target per unit length of trajectory is called the stopping power

usually separated in electronic and nuclear contributions. Nuclear stopping power is primarily important for heavy projectiles with relatively low kinetic energies. Conversely, for fast projectiles the most important energy-loss mechanism is electronic stopping. In this paper, we study the impact of fast light projectiles and, thus, only focus on the electronic stopping power (ESP), which constitutes the first stage of the radiation damage process.

For decades, researchers have been using semiempirical methods based on the dielectric response formalism to study radiobiological effects of ionizing radiation [7], in particular, to calculate the ESP [8–10]. The ESP in such models is defined as

$$S_e(T) = \int_{E_{\min}}^{E_{\max}(T)} E \frac{d\Sigma(E; T)}{dE} dE, \quad (1)$$

where T is the electron incident kinetic energy, E is the electron energy loss, and $d\Sigma/dE$ is the single-differential cross-section (CS), which, in turn, is the integral of the system's energy-loss function (ELF) over momentum q ,

$$\frac{d\Sigma(E; T)}{dE} = \frac{1}{\pi a_0 T} \int_{q_{\min}(E; T)}^{q_{\max}(E; T)} \frac{\text{ELF}(E, q)}{q} dq, \quad (2)$$

where the limits $q_{\min/\max}(E; T) = \sqrt{2m}(\sqrt{T} \mp \sqrt{T - E})$ come from momentum conservation (m is the electron rest mass) [9]. The ELF is a fundamental property of a material

*Corresponding author: natalia.koval.lipina@gmail.com

†Also at the European Research Council Executive Agency (ERCEA). The information and views set out in this article are those of the author and do not necessarily reflect the official opinion of the ERCEA.

Published by the American Physical Society under the terms of the Creative Commons Attribution 4.0 International license. Further distribution of this work must maintain attribution to the author(s) and the published article's title, journal citation, and DOI.

defined as the imaginary part of the inverse macroscopic dielectric function $\text{ELF} = \text{Im}[-1/\epsilon(E, \mathbf{q})]$ [11]. Much of the effort of researchers in the radiobiology community is directed toward accurate modeling of ϵ . Many different models have been suggested to describe the dielectric function and its dependence on q , such as the Drude, Lindhard, and Mermin models, to name but a few, but the optical-data models based on experimental data are state of the art [12]. The dielectric function in the optical-data models is extracted from the optical absorption experimental data (zero momentum transfer). Such models use theoretical extension algorithms to extend the optical data to finite q . Different extension models have been suggested (see review by Nikjoo *et al.* [12]), and among those, Penn [13], Emfietzoglou-Cucinotta-Nikjoo [9], and Mermin energy-loss-function (MELF) [14] models better reproduce the experimental ELF at $q \neq 0$.

Approximations for $q > 0$ make the results for the CSs and ESP uncertain at lower energies, especially below a few hundred eV. Since the q_{\min} in Eq. (2) increases with decreasing T , at lower electron energies, the CSs mostly depend on high-momentum ELF based on extension models, which provide uncertain results, especially below 100 eV, and do not agree with each other [12]. Some recent efforts toward an accurate description of low-energy electron impact on water were made by Emfietzoglou and co-workers [15,16]. In these works, the authors extend the MELF model to include electron-electron interaction by introducing exchange-correlation effects, which improved the agreement with experimental electron inelastic mean free path (inverse total inelastic CS) at energies below 100 eV.

At high proton and electron velocities, the ESP can be well described by linear-response theory. However, the linear description is no longer applicable when the particles travel at intermediate and low velocities (around the Bragg peak and lower) [17]. Moreover, for light particles at sufficiently low velocities, e.g., electrons towards the end of the track, nuclear stopping, and quantum effects become relevant.

Recent developments in density functional theory (DFT) and its time-dependent extension (TDDFT) have advanced significantly the description of the electronic stopping processes in materials in the whole range of velocities [18]. Most of the studies are focused on solid-state materials [19–24], although, some *ab initio* simulations for protons in liquid water became available in recent years. Real-time (RT-)TDDFT calculations of the proton stopping in water, ice, and water vapor provide accurate results and show a quantitative agreement with available experiments [25–27].

Liquid water is commonly used as a target in semiempirical calculations relying on experimental data not available for DNA components. For electrons in water, no studies addressing the nonlinearity of the electronic stopping processes are available to date. However, understanding the nonlinear effects in the interaction of electrons with water is of great importance for benchmarking semiempirical methods and for providing access to the low-energy region in which the dielectric response formalism is not expected to be valid [17]. Hence, in this paper, we present a detailed analysis of the nonlinear effects in the ESP for negative and positive projectiles representing electrons, protons, and muons in water calculated using RT-TDDFT. We compare our results with

dielectric-response calculations and other available data, such as SRIM [28] and ESTAR [29]. We analyze as well the effect of the projectile charge, the so-called Barkas effect [30], on the electronic stopping.

II. METHODOLOGY AND NUMERICAL DETAILS

We used the RT-TDDFT implementation of the open-source SIESTA code [22,31] to evolve the electronic orbitals in time as implemented in version master-post-4.1-264, available in Ref. [32]. In SIESTA, the time-dependent Kohn-Sham (KS) equations are solved by real-time propagation of the KS orbitals using the Crank-Nicolson scheme [33] as recently implemented by Halliday and Artacho [34,35]. The new implementation replaces the Sankey integrator [36] known to be problematic at high energies [37]. The forces on the nuclei of the target atoms and on the projectile itself are disregarded in the time propagation, thereby, describing electron dynamics with frozen host nuclei and a constant velocity projectile as performed in many similar studies [19,20,22,26]. In this way, we can separate the electronic and nuclear contributions to the total stopping and only consider the ESP with a clear velocity dependence. The ESP $S_e = dE_{\text{KS}}(x)/dx$ is obtained from a linear fit of the KS total electronic energy $E_{\text{KS}}(x)$ with respect to the projectile displacement x , along the constant-velocity path. This expression is known to give the correct value of S_e within the density-functional theory defined by the chosen exchange-correlation functional as long as it is an adiabatic one [18,38].

The water samples and the projectile trajectories are as of Gu *et al.* [26]. The simulation cell consisted of 203 water molecules. A total of seven trajectories were considered for each projectile. Gu *et al.* [26] showed that with a limited number of rigorously chosen trajectories it is possible to reproduce accurately the statistically averaged experimental ESP.

The electronic ground state of the target water sample was calculated using the static DFT implementation of the SIESTA code [39] using periodic boundary conditions. For each trajectory, the projectile was placed at the initial position in DFT calculations. We used the generalized gradient approximation in the Perdew, Burke, and Ernzerhof form for the exchange-correlation functional [40]. Norm-conserving Troullier-Martins [41] relativistic pseudopotentials were used to represent the core electrons. The valence electrons were represented by a triple- ζ polarized (TZP) basis set of numerical atomic orbitals with the default energy shift of 0.02 Ry [42]. The electronic Brillouin zone was sampled at the Γ point. The real-space grid was determined by a plane-wave cutoff of 1000 Ry. The KS states were then evolved in time by performing the RT-TDDFT calculations for each projectile moving with different velocities using the time step of 1 as. The convergence of S_e with respect to the time step and the Brillouin zone sampling was tested in Ref. [34].

The point-charge projectiles were modeled via a spherical Gaussian charge distribution, using a SIESTA feature that allows the modeling of charged objects of different shapes. [44]. The parameters defining the Gaussian charge distribution were determined from the comparison of the ESP for a proton projectile moving with the velocity of 1.71 a.u.

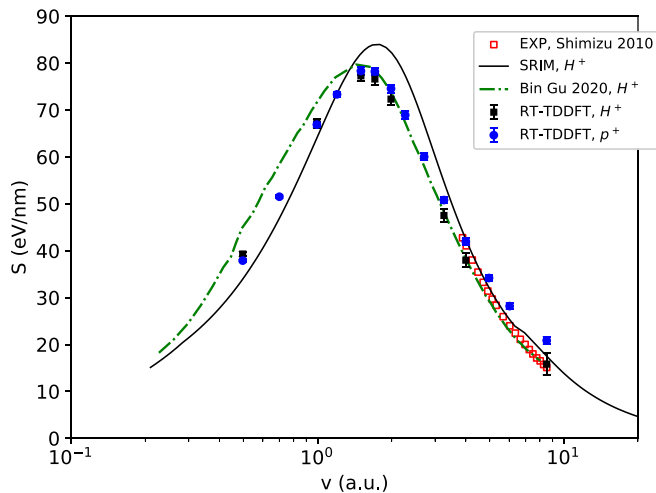


FIG. 1. ESP for a proton in liquid water as a function of velocity. Our results are presented for both the point charge p^+ and the hydrogen ion H^+ (full symbols) and are compared with the SRIM data [28] (solid line), the RT-TDDFT results from Gu *et al.* [26] for H^+ (dashed-dot line), and experimental data from Shimizu *et al.* [43] (empty symbols). The error bars of the RT-TDDFT results depict the accuracy of the linear fit.

($\hbar = e = m_e = 1$) and modeled both as an explicit hydrogen atom and via a Gaussian charge distribution [45], taking the latter as a reference. We determined that the Gaussian positive charge (p^+) distribution given by a width of $\sigma = 0.05 \text{ \AA}$, and a cutoff of 0.5 \AA leads to the same stopping power within 2% as the hydrogen projectile (H^+) as can be seen in Fig. 1. The basis set for the projectile was provided by a ghost hydrogen atom. We used a triple- ζ doubly polarized (TZ2P) basis set on the projectile with cutoff radii $r(\zeta_1) = 8.80$, $r(\zeta_2) = 6.853$,

and $r(\zeta_3) = 0.50$ Bohr for electrons to adapt to the narrow Gaussian distribution. The dependence of S_e on the Gaussian charge width is discussed in the Appendix.

The agreement between our results and Gu *et al.* [26] for H^+ is very reasonable although, at low proton velocities, our ESP is slightly lower than the reference result. The discrepancy may be associated with the differences in the pseudopotentials and basis sets used in our SIESTA calculations, versus the ones used with the CP2K code by Gu *et al.* [26], and with the fact that they performed all-electron calculations. The ESP for p^+ and H^+ from SIESTA RT-TDDFT obtained in this paper and shown in Fig. 1 are in close agreement with each other except for the highest velocities where the p^+ results are slightly higher than the rest of the data sets. The discrepancy mainly comes from the use of different basis sets for the two projectiles, the TZP basis set for the H^+ and the TZ2P one for the ghost atom moving with p^+ . The stopping power is more sensitive to the choice of the basis set at high velocities for both projectiles as our test calculations have shown. As stated before, the Gaussian charge demands more basis than the pseudoised proton.

III. RESULTS AND DISCUSSION

Figure 2(a) shows the comparison of our RT-TDDFT stopping power for a negative point charge (an electron) with the ESP obtained using semiempirical methods by Garcia-Molina *et al.* [46], Emfietzoglou *et al.* [9] and Muñoz *et al.* [48] (theory combined with experiment). Our results are also compared to the dielectric model developed by Ashley *et al.* [49], and the ESTAR [29] data based on Bethe theory. The LR-TDDFT result also presented in Fig. 2(a) is obtained from the *ab initio* energy-loss function [47].

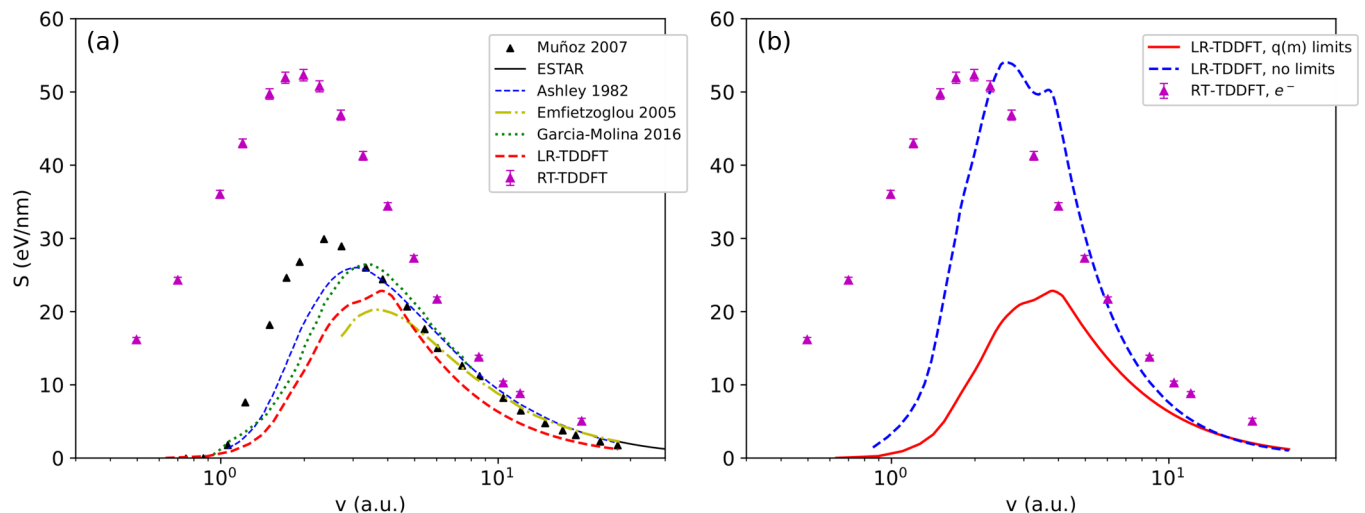


FIG. 2. (a) ESP for an electron in liquid water as a function of velocity calculated with RT-TDDFT compared with the results obtained using the dielectric response formalism from Emfietzoglou *et al.* [9] (dashed-dot line), Gracia-Molina *et al.* [46] (dotted line) and with the LR-TDDFT stopping power [47] (dashed line). The semiempirical data points from Muñoz *et al.* [48] are obtained by converting the mass stopping power for gas phase to ESP by assuming the density of 1 g/cm^3 . ESTAR data [29] (thin solid line, on the most right) and Ashley *et al.* [49] (based on dielectric response, thin dashed line) are also presented for comparison. (b) Comparison of ESP obtained from RT-TDDFT (full symbols) and from LR-TDDFT using the mass-dependent integration limits for q (see Ref. [47]) (solid line) and without such limits (dashed line). See the text for explanation.

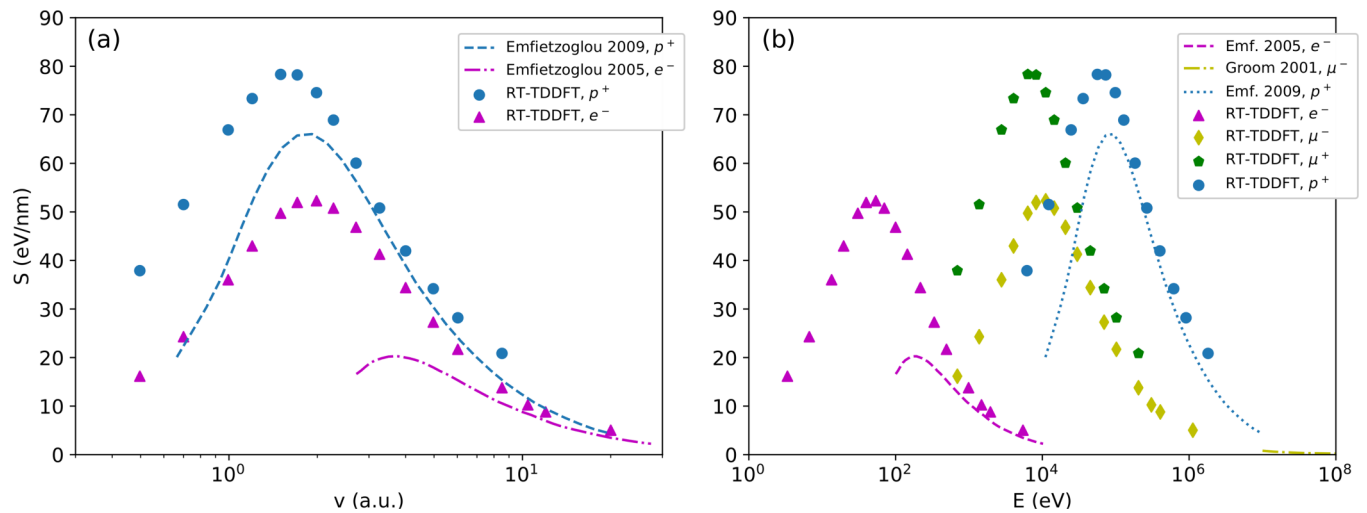


FIG. 3. (a) ESP for a proton and an electron in liquid water as a function of velocity obtained in this paper within RT-TDDFT (full symbols) compared with the dielectric response results from Refs. [9,10] (lines). (b) ESP for an electron, a muon (both negative and positive), and a proton in liquid water as a function of the projectile kinetic energy from RT-TDDFT (full symbols) compared with the dielectric response results for e^- [9] (dashed line) and p^+ [10] (dotted line), and Bethe-Bloch formula for μ^- [50] (dashed-dot line).

We can observe from Fig. 2(a) that all the methods, including linear-response and real-time TDDFT results, agree in the limit of high velocities (above ~ 8 a.u.). This is expected since at high v , the projectile acts as a small perturbation to the system, which have no time to respond to the fast-moving particle and, hence, the process enters linear regime. Below 8 a.u., is where the discrepancy between the linear-response and nonlinear results is remarkable. In particular, the position of the Bragg peak is significantly different. The linear results show a maximum at around 3 to 4 a.u. (energy of the order of 100–200 eV), whereas, the RT-TDDFT gives us the maximum stopping at the velocity of 2 a.u. (~ 50 eV). Slightly closer to ours is the position of the Bragg peak obtained by Muñoz *et al.* [48]. These data points are calculated using experimental cross sections for gas-phase water.

Apart from the large discrepancy between the position of the Bragg peak in the linear and nonlinear stopping power for electrons observed in Fig. 2(a), the maximum value of the ESP is also drastically different. The linear results largely underestimate the stopping power in a wide range of velocities as compared to our *ab initio* nonlinear ESP. A significant part of the discrepancy, however, stems from finite-projectile-mass effects as follows.

Since we use a constant velocity approximation for the electron in our RT-TDDFT calculations, this implies that its mass is infinite. In the linear calculations based on the integration of the electron ELF, although the approximation is built for a constant velocity perturbation, the electron mass is accounted for in the integration limits for the momentum transfer q in Eq. (2). Removing such integration limits for q , and, thus, integrating from zero to infinity over the momentum transfer, we obtain the infinite-mass linear-response ESP. This leads to a much higher ESP as can be seen in Fig. 2(b) (dashed line). Both RT-TDDFT and LR-TDDFT stopping power for infinite electron mass have peaks of similar height. However, the nonlinear effect is still noticeable as the Bragg peak position of the RT-TDDFT ESP is shifted by approximately 1 a.u. of velocity. The comparison in Fig. 2(b)

emphasizes that a constant velocity is a crude approximation for an electron. In a realistic scenario, particularly, at projectile energies below the Bragg peak, disregarding the slowing down of the electron projectile can be a strong approximation. Moreover, at certain conditions, the electron can be completely stopped and captured by the target nuclei. The latter can happen for some trajectories (close impact) but not for others. On average, over many trajectories, the result may be different from our constant-velocity results. The rate of the difference is only possible to predict with a thorough investigation involving a large number of incident velocities and trajectories. Furthermore, at variable electron velocity, extraction of velocity-dependent stopping power becomes a challenging task.

Figure 3(a) shows that the maximum of the ESP for p^+ is higher than for e^- obtained with RT-TDDFT, a phenomenon known as the Barkas effect [30]. Note that the Barkas effect is typically described in relation to projectiles with opposite charges and identical masses, but in this paper, all constant-velocity projectiles have the same (infinite) mass. The position of the maxima (the Bragg peaks), however, is very similar ($v = 1.7$ and 2 a.u. for proton and electron, respectively). This is not true in the case of the results of Emfietzoglou *et al.* in which the Bragg peak is observed at 2 a.u. for the proton and at 4 a.u. for the electron projectile. Overall, the linear-nonlinear discrepancy is much more pronounced for electron projectiles.

Figure 3(b) shows the ESP for an electron, a negative, a positive muon, and a proton as a function of the projectile kinetic energy. For the positive (negative) muon, we used the results of the proton (electron) scaling the kinetic energy taking into account the muon mass $M_\mu = 206.768m_e$ [51]. The Bragg peak is at energies of ~ 50 eV, 10, and 90 keV for the electron, muons, and proton, respectively. The Bragg peak energies scale linearly with the masses of the three particles (e.g. for a proton vs muon $M_p/M_\mu = 8.88m_e$) as expected since their only mass dependence arises from the velocity-energy conversion. The mass dependence is not linear in the

case of the dielectric-response model of Refs. [9,10] in which the mass is explicitly included in the method. For a negative muon, the Bethe-Bloch result [50] is only available at energies above 10^7 eV, out of range of our calculations.

IV. CONCLUSIONS

In conclusion, we presented the electronic stopping power for negative and positive projectiles in liquid water obtained with RT-TDDFT and compared to linear results available in the literature. Correcting for projectile mass effects, the nonlinear effects have been shown to be prominent in the electron-water interaction given the large difference between the linear and nonlinear ESP. This effect, however, has to be verified by calculations considering the quantum nature of the external electron and accounting properly for its finite mass.

ACKNOWLEDGMENTS

We acknowledge funding from the Research Executive Agency under the European Union’s Horizon 2020 Research and Innovation Program (Project No. ESC2RAD: Enabling Smart Computations to study space RADIation effects, Grant Agreement No. 776410). J.K. was supported by the Beatriz Galindo Program (BEAGAL18/00130) from the Ministerio de Educación y Formación Profesional of Spain, and by the Comunidad de Madrid through the Convenio Plurianual with Universidad Politécnica de Madrid in its line of action Apoyo a la realización de proyectos de I+D para investigadores Beatriz Galindo within the framework of V PRICIT (V Plan Regional de Investigación Científica e Innovación Tecnológica). E.A. acknowledges the funding from Spanish MINECO through Grant No. FIS2015-64886-C5-1-P, and from Spanish MICIN through Grant No. PID2019-107338RB-C61/AEI/10.13039/501100011033, as well as a María de Maeztu award to Nanogune, Grant No. CEX2020-001038-M funded by MCIN/AEI/10.13039/501100011033. We are grateful for computational resources provided by the Donostia International Physics Center (DIPC) Computer Center and Barcelona Supercomputer Center (BSC HPC Projects No. FI-2021-2-0037 and No. FI-2021-3-0030).

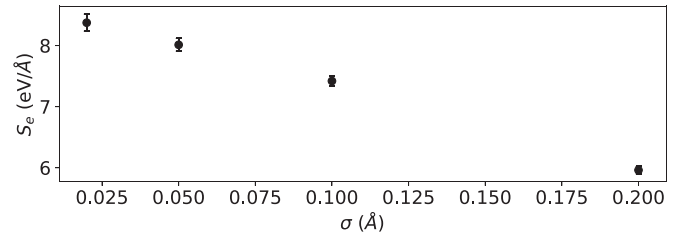


FIG. 4. Electronic stopping power (in eV/Å) for a proton in liquid water as a function of the width σ (in angstroms) of the spherical Gaussian used to represent the proton charge for a proton velocity of 1.71 a.u. The error bars of the RT-TDDFT results depict the accuracy of the linear fit for extracting the stopping power.

APPENDIX: PROJECTILE CHARGE WIDTH

As already known from earlier work [19], the electronic stopping power depends on the smoothening of the Coulomb interaction of the projectile with the system electrons at short distances. Such smoothening is performed both when using pseudopotentials and when substituting a point charge by a charge distribution. Our test results have shown that indeed the width of the Gaussian affects the stopping power in the calculations in this paper. Namely, as could be expected, the ESP increases as the Gaussian becomes narrower (see Fig. 4).

The limit of zero width does not represent a convergence target, however, since the projectile is not a classical point charge. It could be argued that such a width should scale with the de Broglie wavelength.

From a technical point of view, such a width should not be smaller [19] than the discretization of real space used to compute the Hamiltonian matrix elements and specified by the plane-wave energy cutoff [39] of 1000 Ry in this paper, which implies a half wavelength of 0.1 Bohr. We chose to use the same Gaussian width for the whole range of velocities, obtained from reproducing the Bragg peak values obtained with the explicit all-electron calculations in Ref. [26] for the electronic stopping power for protons. We, then, used the same width to model the negatively charged Gaussian-distributed projectiles.

[1] O. Jäkel, Physical advantages of particles: protons and light ions, *Br. J. Radiol.* **93**, 20190428 (2020).

[2] F. Tommasino and M. Durante, Proton radiobiology, *Cancers* **7**, 353 (2015).

[3] F. Ferrari and E. Szuskiewicz, Cosmic rays: A review for astrobiologists, *Astrobiology* **9**, 413 (2009).

[4] M. Durante and F. A. Cucinotta, Physical basis of radiation protection in space travel, *Rev. Mod. Phys.* **83**, 1245 (2011).

[5] M. Maalouf, M. Durante, and N. Foray, Biological effects of space radiation on human cells: History, advances and outcomes, *J. Radiat. Res.* **52**, 126 (2011).

[6] L. Walsh, U. Schneider, A. Fogtman, C. Kausch, S. McKenna-Lawlor, L. Narici, J. Ngo-Anh, G. Reitz, L. Sabatier, G. Santin, L. Sihver, U. Straube, U. Weber, and M. Durante, Research plans in Europe for radiation health hazard assessment in exploratory space missions, *Life Sci. Space Res.* **21**, 73 (2019).

[7] K. P. Chatzipapas, P. Papadimitroulas, D. Emfietzoglou, S. A. Kalospyros, M. Hada, A. G. Georgakilas, and G. C. Kagadis, Ionizing radiation and complex DNA damage: Quantifying the radiobiological damage using monte carlo simulations, *Cancers* **12**, 799 (2020).

[8] Z. Francis, S. Incerti, M. Karamitros, H. Tran, and C. Villagrasa, Stopping power and ranges of electrons, protons and alpha particles in liquid water using the Geant4-DNA package, *Nucl. Instrum. Methods Phys. Res., Sect. B* **269**, 2307 (2011).

[9] D. Emfietzoglou, F. A. Cucinotta, and H. Nikjoo, A complete dielectric response model for liquid water: A solution of the Bethe Ridge problem, *Radiat. Res.* **164**, 202 (2005).

[10] D. Emfietzoglou, R. Garcia-Molina, I. Kyriakou, I. Abril, and H. Nikjoo, A dielectric response study of the electronic stopping power of liquid water for energetic protons and a new I-value for water, *Phys. Med. Biol.* **54**, 3451 (2009).

- [11] D. Emfietzoglou, Inelastic cross-sections for electron transport in liquid water: a comparison of dielectric models, *Radiat. Phys. Chem.* **66**, 373 (2003).
- [12] H. Nikjoo, D. Emfietzoglou, T. Liamsuwan, R. Taleei, D. Liljequist, and S. Uehara, Radiation track, DNA damage and response—a review, *Rep. Prog. Phys.* **79**, 116601 (2016).
- [13] D. R. Penn, Electron mean-free-path calculations using a model dielectric function, *Phys. Rev. B* **35**, 482 (1987).
- [14] I. Abril, R. Garcia-Molina, C. D. Denton, F. J. Pérez-Pérez, and N. R. Arista, Dielectric description of wakes and stopping powers in solids, *Phys. Rev. A* **58**, 357 (1998).
- [15] D. Emfietzoglou, I. Kyriakou, R. Garcia-Molina, I. Abril, and H. Nikjoo, Inelastic cross sections for low-energy electrons in liquid water: Exchange and correlation effects, *Radiat. Res.* **180**, 499 (2013).
- [16] D. Emfietzoglou, I. Kyriakou, R. Garcia-Molina, and I. Abril, Inelastic mean free path of low-energy electrons in condensed media: beyond the standard models, *Surf. Interface Anal.* **49**, 4 (2017).
- [17] A. A. Shukri, F. Bruneval, and L. Reining, *Ab initio* electronic stopping power of protons in bulk materials, *Phys. Rev. B* **93**, 035128 (2016).
- [18] A. A. Correa, Calculating electronic stopping power in materials from first principles, *Comput. Mater. Sci.* **150**, 291 (2018).
- [19] J. M. Pruneda, D. Sánchez-Portal, A. Arnau, J. I. Juaristi, and E. Artacho, Electronic Stopping Power in LiF from First Principles, *Phys. Rev. Lett.* **99**, 235501 (2007).
- [20] M. A. Zeb, J. Kohanoff, D. Sánchez-Portal, A. Arnau, J. I. Juaristi, and E. Artacho, Electronic Stopping Power in Gold: The Role of *d* Electrons and the H/He Anomaly, *Phys. Rev. Lett.* **108**, 225504 (2012).
- [21] A. Schleife, Y. Kanai, and A. A. Correa, Accurate atomistic first-principles calculations of electronic stopping, *Phys. Rev. B* **91**, 014306 (2015).
- [22] R. Ullah, F. Corsetti, D. Sánchez-Portal, and E. Artacho, Electronic stopping power in a narrow band gap semiconductor from first principles, *Phys. Rev. B* **91**, 125203 (2015).
- [23] I. Maliyov, J.-P. Crocombette, and F. Bruneval, Electronic stopping power from time-dependent density-functional theory in Gaussian basis, *Eur. Phys. J. B* **91**, 172 (2018).
- [24] N. E. Koval, F. Da Pieve, and E. Artacho, *Ab initio* electronic stopping power for protons in $\text{Ga}_{0.5}\text{In}_{0.5}\text{P}/\text{GaAs}/\text{Ge}$ triple-junction solar cells for space applications, *R. Soc. Open Sci.* **7**, 200925 (2020).
- [25] K. G. Reeves, Y. Yao, and Y. Kanai, Electronic stopping power in liquid water for protons and α particles from first principles, *Phys. Rev. B* **94**, 041108(R) (2016).
- [26] B. Gu, B. Cunningham, D. Muñoz Santiburcio, F. Da Pieve, E. Artacho, and J. Kohanoff, Efficient *ab initio* calculation of electronic stopping in disordered systems via geometry pre-sampling: Application to liquid water, *J. Chem. Phys.* **153**, 034113 (2020).
- [27] B. Gu, D. Muñoz-Santiburcio, F. Da Pieve, F. Cleri, E. Artacho, and J. Kohanoff, Bragg’s additivity rule and core and bond model studied by real-time TDDFT electronic stopping simulations: The case of water vapor, *Radiat. Phys. Chem.* **193**, 109961 (2022).
- [28] J. F. Ziegler, M. Ziegler, and J. Biersack, SRIM—The stopping and range of ions in matter, *Nucl. Instrum. Methods Phys. Res., Sect. B* **268**, 1818 (2010).
- [29] M. Berger, J. Coursey, M. Zucker, and J. Chang, ESTAR, PSTAR, and ASTAR: Computer programs for calculating stopping-power and range tables for electrons, protons, and helium ions, <http://physics.nist.gov/Star>.
- [30] W. H. Barkas, J. N. Dyer, and H. H. Heckman, Resolution of the σ -Mass Anomaly, *Phys. Rev. Lett.* **11**, 26 (1963).
- [31] A. Tsolakidis, D. Sánchez-Portal, and R. M. Martin, Calculation of the optical response of atomic clusters using time-dependent density functional theory and local orbitals, *Phys. Rev. B* **66**, 235416 (2002).
- [32] SIESTA Project, <https://gitlab.com/npapior/siesta/-/tree/geometry-motion>.
- [33] J. Crank and P. Nicolson, A practical method for numerical evaluation of solutions of partial differential equations of the heat-conduction type, *Math. Proc. Cambridge Philos. Soc.* **43**, 50 (1947).
- [34] J. F. K. Halliday and E. Artacho, Anisotropy of electronic stopping power in graphite, *Phys. Rev. B* **100**, 104112 (2019).
- [35] J. F. K. Halliday and E. Artacho, Numerical integration of quantum time evolution in a curved manifold, *Phys. Rev. Res.* **3**, 043134 (2021).
- [36] J. K. Tomfohr and O. F. Sankey, Time-dependent simulation of conduction through a molecule, *Phys. Status Solidi B* **226**, 115 (2001).
- [37] E. Artacho and D. D. O’Regan, Quantum mechanics in an evolving hilbert space, *Phys. Rev. B* **95**, 115155 (2017).
- [38] J. F. K. Halliday, M. Famili, N. Forcellini, and E. Artacho, *Ab initio* electronic stationary states for nuclear projectiles in solids, *Phys. Rev. Res.* **4**, 043077 (2022).
- [39] J. M. Soler, E. Artacho, J. D. Gale, A. García, J. Junquera, P. Ordejón, and D. Sánchez-Portal, The SIESTA method for *ab initio* order-*N* materials simulation, *J. Phys.: Condens. Matter* **14**, 2745 (2002).
- [40] J. P. Perdew, K. Burke, and M. Ernzerhof, Generalized Gradient Approximation Made Simple, *Phys. Rev. Lett.* **77**, 3865 (1996).
- [41] N. Troullier and J. L. Martins, Efficient pseudopotentials for plane-wave calculations, *Phys. Rev. B* **43**, 1993 (1991).
- [42] E. Artacho, D. Sánchez-Portal, P. Ordejón, A. García, and J. M. Soler, Linear-scaling *ab-initio* calculations for large and complex systems, *Phys. Status Solidi B* **215**, 809 (1999).
- [43] M. Shimizu, T. Hayakawa, M. Kaneda, H. Tsuchida, and A. Itoh, Stopping cross-sections of liquid water for 0.3–2.0 MeV protons, *Vacuum* **84**, 1002 (2010).
- [44] N. Papior, T. Gunst, D. Stradi, and M. Brandbyge, Manipulating the voltage drop in graphene nanojunctions using a gate potential, *Phys. Chem. Chem. Phys.* **18**, 1025 (2016).
- [45] The additional electron implied by a H atom vs a proton does not perceptibly affect the final result in a large enough sample.
- [46] R. Garcia-Molina, I. Abril, I. Kyriakou, and D. Emfietzoglou, Inelastic scattering and energy loss of swift electron beams in biologically relevant materials, *Surf. Interface Anal.* **49**, 11 (2017).
- [47] N. E. Koval, P. Koval, F. Da Pieve, J. Kohanoff, E. Artacho, and D. Emfietzoglou, Inelastic scattering of electrons in water from first principles: cross sections and inelastic mean free path

- for use in monte carlo track-structure simulations of biological damage, *R. Soc. Open Sci.* **9**, 212011 (2022).
- [48] A. Muñoz, J. C. Oller, F. Blanco, J. D. Gorfinkiel, P. Limão-Vieira, and G. García, Electron-scattering cross sections and stopping powers in H₂O, *Phys. Rev. A* **76**, 052707 (2007).
- [49] J. C. Ashley, Stopping power of liquid water for low-energy electrons, *Radiat. Res.* **89**, 25 (1982).
- [50] D. E. Groom, N. V. Mokhov, and S. I. Striganov, Muon stopping power and range tables 10 MeV–100 TeV, *At. Data Nucl. Data Tables* **78**, 183 (2001).
- [51] U.S. National Institute of Standards and Technology. Fundamental Physical Constants from NIST, <https://physics.nist.gov/cuu/Constants/index.html>.